

This is an Open Access document downloaded from ORCA, Cardiff University's institutional repository:<https://orca.cardiff.ac.uk/id/eprint/114446/>

This is the author's version of a work that was submitted to / accepted for publication.

Citation for final published version:

Mattos, Nathalia, Alves, Tiago and Scully, Aisling 2018. Structural and depositional controls on Plio-Pleistocene submarine channel geometry (Taranaki Basin, New Zealand). *Basin Research* 31 (1) , pp. 136-154. 10.1111/bre.12312

Publishers page: <https://doi.org/10.1111/bre.12312>

Please note:

Changes made as a result of publishing processes such as copy-editing, formatting and page numbers may not be reflected in this version. For the definitive version of this publication, please refer to the published source. You are advised to consult the publisher's version if you wish to cite this paper.

This version is being made available in accordance with publisher policies. See <http://orca.cf.ac.uk/policies.html> for usage policies. Copyright and moral rights for publications made available in ORCA are retained by the copyright holders.





36 models, in which the development of kinematically related segments result from the upward propagation of a  
37 reactivated fault (Childs et al., 2009; Giba et al., 2012).

38 Relay ramps are structures developed in rift basins that closely control the subaerial and subaqueous influx  
39 of sediment from footwall highs towards hanging-wall depocentres (Athmer et al., 2010; Athmer and Luthi,  
40 2011; Fossen and Rotevatn, 2016; Gawthorpe and Hurst, 1993; Soreghan et al., 1999). Hence, the presence of  
41 relay ramps in tectonically active basins has a significant impact on sediment accommodation space, basin  
42 architecture and, consequently, on the deposition of reservoir units on hanging-wall depocentres (Athmer and  
43 Luthi, 2011; Gawthorpe and Hurst, 1993; Gupta et al., 1999; Ravnås and Steel, 1998). Relay ramps can change  
44 the course of fluvial systems by either obstructing their downslope flow or guiding sediment influx into  
45 alternative paths (Gee et al., 2007; Hopkins and Dawers, 2018). Previous studies have integrated observations  
46 of relay ramps from submarine settings with data from their subaerial (fluvial) to coastal analogues (Anderson  
47 et al., 2000; Athmer and Luthi, 2011; Mulrooney et al. 2018) to show the influence of faulting on the creation  
48 of accommodation space. However, the structural controls on accommodation and syn-rift deposition were  
49 only recently assessed in a submarine setting (Ge et al., 2017; Ge et al., 2018). This work aims at addressing  
50 the role of relay ramps as pathways for turbidity currents in an area with high-quality 3D seismic data.

51 In the Northern Graben of the Taranaki Basin, offshore New Zealand (Figs. 1a and 1b), a set of relay  
52 ramps was formed in the Late Cenozoic between four isolated fault segments of the Parihaka Fault (S1 to S4),  
53 with lengths varying from 8 km to 15 km (Giba et al., 2012). The Parihaka Fault is by itself part of the larger  
54 Cape Egmont Fault Zone and records: a) normal and left-lateral oblique reactivation during the Late  
55 Cretaceous, b) reverse displacement associated with the onset of andesitic volcanism in the Mid-Miocene, and  
56 c) oblique-slip movement during Plio-Pleistocene back-arc extension, which culminated in the opening of the  
57 Northern Graben (Giba et al., 2010; Hansen and Kamp, 2004a; King, 2000; King and Thrasher, 1996, Nodder,  
58 1993) (Figs. 2a and 2b). High sedimentation rates accompanied the reactivation of the Parihaka Fault in the  
59 Plio-Pleistocene and led to the deposition of the Giant Foresets Formation, a thick syn-rift sequence comprising  
60 clinoforms incised by Pleistocene submarine channels (King and Thrasher, 1996; Salazar et al., 2016) (Fig.  
61 2c).

62 This study investigates the control relay ramps exerted on the deposition of Late Pliocene strata in the  
63 Northern Graben, where laterally and vertically stacked submarine channels are identified within the Giant  
64 Foresets Formation (Fig. 2c). The identification of different drainage types in the Parihaka 3D seismic volume  
65 is complemented with the interpretation of channel geometries, reservoir prediction within channelised units,  
66 and by addressing the influence of the relay ramps on depositional systems in the Taranaki Basin. The  
67 relationship between different drainage types and regional faulting, as established in this work, will contribute  
68 to a more complete understanding of how fault systems control submarine channel geometries.

69

## 70 **2. Geological Setting**

71

72 The Taranaki Basin is a Cretaceous-Holocene asymmetric basin located to the west of New Zealand over  
73 an area of ~100.000 km<sup>2</sup> (King and Thrasher, 1996). The Taranaki Fault bounds the Taranaki Basin to the east

74 (Holt and Stern, 1991) (Fig. 1a). The western and southern limits of the Taranaki Basin are, respectively, the  
75 Challenger Plateau and the sub-basins of the South Island (Fig. 1a). To the northwest of the study area, the  
76 Taranaki Basin terminates in the New Caledonian Basin (King and Thrasher, 1996).

77 The Cape Egmont Fault Zone divides the Taranaki Basin into the relatively undeformed Western Stable  
78 Platform and the tectonically active Eastern Mobile Belt (King and Thrasher, 1996; Nodder, 1993) (Fig. 1b).  
79 The Eastern Mobile Belt comprises a Northern Graben, a Central Graben, and the buried Miocene Mohakatino  
80 Volcanic Centre (Hansen and Kamp, 2004a; Neall et al., 1986; Stagpoole and Funnell, 2001). The complex  
81 deformation history of the Eastern Mobile Belt includes extensional episodes that were concomitant with basin  
82 subsidence, and compression between the Australian and Pacific plates occurring from Late Cretaceous to  
83 Early Eocene (Giba et al., 2010; Holt and Stern, 1991; Holt and Stern, 1994; King and Thrasher, 1996; Nicol  
84 et al., 2005; Stagpoole and Nicol, 2008).

85 Oligocene subsidence chiefly affected the eastern part of the Taranaki Basin. During the earliest Miocene,  
86 basin subsidence gave way to compression resulting from westward thrusting along the Taranaki Fault (Kamp  
87 et al., 2004a; Kamp et al., 2004b; King, 2000; King and Thrasher, 1996; Nicol et al., 2004). Andesitic volcanic  
88 complexes were active in the Taranaki Basin from ~ 12 Ma to 6 - 4.8 Ma, resulting in the formation of the  
89 Mohakatino Volcanic Centre (Hansen and Kamp, 2004a). A high degree of uncertainty for the ages of  
90 volcanism in the Taranaki Basin results from the absence of continuously cored boreholes; these would allow  
91 the identification of stratal relations between volcanic and sedimentary units (Hansen and Kamp, 2004a).

92 Shortening in the south and extension in the north of the Taranaki Basin occurred concomitantly from the  
93 Miocene to the Plio-Pleistocene (Giba et al., 2010; Holt and Stern, 1994; Stagpoole and Nicol, 2008). Back-  
94 arc extension during the Early Pliocene led to the formation of the Northern Graben, an NNE-SSW fan-shaped  
95 graben delimited by the Cape Egmont Fault Zone to the west and by the Turi Fault Zone to the east (Giba et  
96 al., 2010; King, 2000; King and Thrasher, 1996) (Fig. 1b).

97 The Cape Egmont Fault Zone extends for more than 200 km along the western portion of the Taranaki  
98 Basin, comprising normal, reverse and *en echelon* faults (King and Thrasher, 1996; Nodder, 1993). The  
99 Parihaka Fault is one of the main structures of the Cape Egmont Fault Zone, consisting of four individual fault  
100 segments (S1 to S4 from south to north, Fig. 2a) that are 8 km to 15 km long, for a total length of approximately  
101 50 km (Giba et al., 2012) (Figs. 1b and 2a). The southern segments of the Cape Egmont Fault Zone (S1 and  
102 S2) are hard-linked at Late Cretaceous level (Figs. 2b and 2c). Early Pliocene (3.7 Ma) back-arc extension  
103 reactivated segments S1 and S2 with a maximum vertical displacement of 600 m and, at the same time, formed  
104 the NE-striking segments to the north of the Cape Egmont Fault Zone (S3 and S4, Fig. 1b).

105 The reactivation of segments S1 and S2 ceased during the Pleistocene, whilst segments S3 and S4  
106 continued to propagate in the Holocene, resulting in vertical displacements of up to 1450 m for segment S4  
107 (Giba et al., 2012). Relay ramps were developed between segments S3 and S4 according to the coherent fault  
108 growth model of Walsh et al. (2003) (Fig. 2a). Thus, variations in fault strikes resulted in important rotation  
109 of the fault surface, producing a three-dimensional sigmoidal shape in cross-section (Fig. 2c). The growth of  
110 the Parihaka Fault along segments S3 and S4 was accommodated by later displacement and rotation of relay  
111 zones (Giba et al., 2012).

112 The Miocene – Quaternary stratigraphy of the Taranaki Basin is shown in detail in Figure 3. Miocene  
113 units are associated with the regressive Wai-ti Group and volcanoclastic sediments from the Mohakatino  
114 Formation (King and Thrasher, 1996). In the Northern Graben, the Plio-Pleistocene Rotokare Group includes  
115 prograding fan deposits of the basal Mangaa Formation, plus shelf and slope sediments of the Giant Foresets  
116 Formation (Hansen and Kamp, 2002). The studied interval is part of the Giant Foresets Formation, a ~2000  
117 m-thick unit comprising fine sands and muds, characterised on seismic data by the presence of clinofolds and  
118 incised submarine channels (Hansen and Kamp, 2002, King and Thrasher, 1996; Salazar et al., 2016). High  
119 sedimentation rates recorded within the Giant Foresets Formation were responsible for preserving the growth  
120 history of the Parihaka Fault segment during the Plio-Pleistocene (King and Thrasher, 1996).

121

### 122 3. Data and Methods

123

#### 124 3.1. Dataset

125 The Parihaka 3D volume covers a total area of 1,520 km<sup>2</sup> of the Taranaki Basin, at a maximum water depth  
126 of 150 m (Fig. 1b). The study area corresponds to a polygon with 705 km<sup>2</sup> around the Parihaka Fault segments  
127 (Fig. 2a). The zero-phased seismic dataset was acquired with an 8 x 4500 m array of streamers and later  
128 resampled at 4 ms TWT intervals. High-resolution Radon Transform linear noise attenuation, TAU-P domain  
129 deconvolution, and NMO corrections to the 60-fold coverage of the seismic trace preceded the processing of  
130 the seismic volume. A Kirchhoff time migration algorithm was then applied to 1 km grids. The final output is  
131 a stacked data volume with 12.5 x 12.5 m bins. Interpreted seismic profiles are displayed in normal SEG  
132 convention, with amplitude peaks shown in red and amplitude troughs in blue (see inset on Fig. 2c).

133 Well Arawa-1 was plugged and abandoned in the centre of the Parihaka 3D volume, and reached total depth  
134 of 3055 m (Arco, 1992). A dominant frequency of 40 Hz and an average velocity of 2000 m/s for the Plio-  
135 Pleistocene interval (Giba et al., 2012; Salazar et al., 2016) correspond to a vertical resolution of 12.5 m.

#### 136 3.2. Channel interpretation methods

137 Seismic interpretation included fault and horizon mapping in Schlumberger's Petrel<sup>®</sup>. Interpreted horizons  
138 were numbered in chronological order from oldest to youngest, prefixed by the letter H (e.g., H<sub>1</sub>, H<sub>2</sub>, H<sub>3</sub>).  
139 Horizons at the base and top of the main channel section (within H<sub>2</sub> and H<sub>3</sub>) were labelled BC and TC,  
140 respectively (Fig. 2c). Biostratigraphical markers of Crundwell et al. (2004) and Morgans (2006) were used to  
141 correlate the stratigraphic interval of interest, which corresponds to strata with ages ranging from 4.5 to 2.4  
142 Ma (seismic units SU2 and SU5 in Salazar et al., 2016).

143 Time-structural and thickness maps for horizons BC and TC were also generated (Fig. 4). In this work,  
144 velocity data were used to depth-convert the TWT thickness maps. Individual channels and channel complex  
145 systems were identified on seismic profiles as isolated or stacked U- and V- shaped erosional features based  
146 on amplitude contrasts between the channel-fill and its surroundings (Deptuck et al., 2003; Posamentier and  
147 Kolla, 2003).

148 The bounding surfaces of four large-scale submarine channel complex systems (Channel Complex Systems  
149 1-4) were mapped using the procedure described by [Deptuck et al. \(2003\)](#). This procedure consists in the  
150 identification of the lowermost continuous channel incision surface on seismic profiles. Channel complexes  
151 represent groups of discrete submarine channels, while channel complex systems represent confined groups of  
152 channel complexes ([Mayall et al., 2006](#)). Submarine channels' hierarchical frameworks were thus identified  
153 based on: a) the geometry of channel fill strata, b) vertical and lateral channel stacking patterns, and c) the  
154 relative distribution of their bounding surfaces ([Abreu et al., 2003](#); [Clark and Pickering, 1996](#); [Mayall et al.,](#)  
155 [2006](#)). In addition, confined channels tend to exhibit important vertical stacking, whereas sinuous and less  
156 confined channels tend to show lateral stacking ([Abreu et al., 2003](#); [Clark and Pickering, 1996](#)). Distinct  
157 stacking patterns in submarine channels result from gradual to abrupt shifts in their position(s).

158 The Parihaka 3D seismic volume was flattened to remove discontinuities and reveal periods of syn-  
159 depositional fault growth, thus highlighting the relationship between submarine channels and the Parihaka  
160 Fault (*cf.* [Lee, 2001](#); [Lomask, 2003](#)). Faults bounding the relay ramps were identified on the seismic lines as  
161 overlapping, laterally continuous structures ([Long and Imber, 2011](#)) (Fig. 2c). We used horizon TC, with an  
162 estimated age of 2.45 Ma based on foraminifera samples ([Salazar et al., 2016](#)), as the reference horizon to  
163 flatten the seismic volume.

164 Horizon TC post-dates the onset of reactivation of the Parihaka Fault during the Plio-Pleistocene, allowing  
165 us to investigate the influence of this structure on Channel System Complexes 1 and 2. In order to include  
166 Channel System 3 in this analysis, we flattened the seismic cube using the top prograding horizon H<sub>3</sub> (1.26  
167 Ma) as reference, as this channel system incises horizon TC (Fig. 2c).

168 The three-dimensional geometry of channels at depth was investigated using a quantitative approach. The  
169 distribution of channel system complexes was measured in relation to channel points (CP) located at the base  
170 of the channels ([Gamboa et al., 2012](#)) (Fig. 5a). The channel points (CP) method is scale- and survey-  
171 independent, consisting in the plotting of CPs at the base of channels on variance time slices. The maximum  
172 channel width between each sides of the channel complex system, and the maximum channel height measured  
173 from the top to the base of the channel complex system, were computed for each channel point. We used a  
174 spacing of 25 ms TWT between each time slice, at a depth varying between 864 ms and 2616 ms TWT. These  
175 depths correspond to the shallowest and the deepest submarine channels on the variance slices (Figs. 5b – 5e).  
176 The location of the channel points (X, Y, and Z) were exported into ArcMap and gridded using the ordinary  
177 kriging method with a polygon delimiting the study area. A channel point density map based on the overall  
178 spatial arrangement of the CPs was thus created to highlight the degree of variability in channel clustering and  
179 distribution.

180

#### 181 **4. Geometry of the main channel sequence and interaction with the Parihaka Fault segments**

182

183 The interval of interest to this work is bounded at its base and top by horizons BC and TC (Figs. 2c and  
184 4a). It is part of the Giant Foresets Formation (Fig. 3). Horizon BC is a medium- to high-amplitude positive  
185 reflection, continuous on the footwall of the Parihaka Fault, and offset by faults on its hanging-wall (Figs. 2c

186 and 4a). The depth of Horizon BC ranges between 1250 ms and 1500 ms TWT on the footwall block, and  
187 between 2150 ms and 2250 ms TWT on the hanging-wall block, with an overall dip to the E and NE,  
188 respectively (Fig. 4a). Horizon BC correlates with the base of seismic unit SU2 in Salazar et al. (2016), dated  
189 as 4.5 Ma using foraminifera (Morgans, 2006).

190 Horizon TC is a medium- to high-amplitude positive reflection incised by small-scale channel tributaries  
191 and is offset by the Parihaka Fault (Figs. 2c and 4b). The base of horizon TC ranges in depth between 900 ms  
192 and 1050 ms TWT on the footwall block, and 950 ms and 1450 ms TWT on the hanging-wall block (Fig 4b).  
193 It corresponds to the top of the seismic unit SU5 of Salazar et al. (2016), with an assigned age of ~ 2.45 Ma  
194 (Morgans, 2006). The thickness of the main channel sequence, between horizons BC and TC, varies from 350  
195 m to 400 m on the footwall block (Fig. 4c). The thickness of this same interval reaches its lowest value (200 -  
196 250 m) along the discrete Parihaka Fault segments. On the hanging-wall block, two thickness maxima are  
197 observed between horizons BC and TC (500 – 800 m). They are referred herein as depocentres 1 and 2 (Fig.  
198 4c).

199 The interval between BC and TC comprises high-amplitude prograding reflections incised either by single  
200 channel complex sets with a large erosional base, or by multiple basal tributaries with widths up to 1 km. These  
201 tributaries converge to form a large channel complex system (Fig. 6). Channel fill deposits are low- to medium-  
202 amplitude, chaotic and discontinuous reflections (Fig. 6). Evidence for vertical and lateral stacking of the  
203 channel bodies is observed throughout the study area (Fig. 6). Four channel complex systems, named 1 to 4,  
204 were thus identified (Figs. 7 to 10).

205

#### 206 *4.1. Channel Complex System 1*

207

208 Channel Complex System 1 is a ~27 km long conduit offset by segment S1 (Figs. 7a and 7b). This channel  
209 complex system extends beyond the limits of the seismic volume. The erosive base of the channel complex  
210 system is observed on seismic at a maximum depth of 1100 ms TWT below the sea floor. Isolated channels  
211 with widths up to 1 km and thicknesses of up to 200 m are recognised as tributaries to this channel system on  
212 the footwall block (Fig. 6a).

213 Segment S1 shows a horsetail geometry in the southern section (section A-B, Fig. 6a), comprising faults  
214 initiated below horizon BC that propagate to a depth of 1250 ms TWT. Lateral migration at the base of this  
215 channel complex system indicates a deflection of the channel course, and vertically stacked channel complex  
216 deposits are observed on the hanging-wall block (Fig. 6a).

217 The channel complex sets in the central profiles (profiles C-D and E-F; Figs. 6b and 6c) are characterised  
218 by planar to slightly concave-upward basal surfaces in a multistorey (nested) offset stacking arrangement. In  
219 section E-F, Channel Complex System 1 reaches its maximum width (10.4 km), as deposits seem to be less  
220 confined, a character suggesting the deposition of multiple submarine fans. In the northern section, the erosive  
221 base of Channel Complex System 1 is clearer than in section E-F, and multiple planar to slightly concave

222 upward lobate surfaces are observed (section G-H; Fig. 6d). The main channel direction in the footwall block  
223 is SW-NE, with two main branches forming angles of 44° and 65° with respect to segment S1 (Fig. 7a). A third  
224 tributary is perpendicular to the trace of segment S1, whereas the northernmost tributary of Channel Complex  
225 System 1 forms an angle of 85° to this segment (Fig. 7a). This channel system is oblique in relation to S1.  
226 Channel Complex System 1 changes its sinuosity to the SE of the study area, where meandering channels are  
227 observed on the hanging-wall block (Figs. 7a and 7b).

228 Confluence of these branches occurs on the fault-bounded slope, and a single conduit is observed on the  
229 hanging-wall block ranging in width from 0.9 km to 3.3 km. Away from S1, this channel system reaches  
230 thicknesses of up to 350 metres (Fig. 7b), coinciding with the location of Depocentre 1 (Fig. 4c). In the  
231 unflattened seismic section a similar channel-fill reflection pattern, with continuity interrupted by S1, is  
232 observed on both the footwall and hanging-wall blocks (Fig. 7c). In the flattened seismic section, using horizon  
233 TC as a reference, the removal of segment S1 allows the reconstruction of the original position of Channel  
234 Complex System 1, suggesting that reactivation of S1 around 3.7 Ma generated accommodation space on its  
235 immediate hanging-wall block (Fig 7d).

236

#### 237 *4.2. Channel Complex System 2*

238

239 Channel Complex System 2 is a ~15 km-long channel complex system located in the central part of the  
240 study area, within the limits of the Parihaka 3D volume (Fig. 8). The confined base of this channel complex  
241 system initially forms an angle of 61° to the NNE-striking segment S2 on the footwall block. It then forms a  
242 perpendicular angle to S2 on the hanging-wall block (Figs. 8a and 8b). This channel system is thus classified  
243 as being transverse to S2. Channel orientation downdip varies from SW-NE to W-E, adjacent to S2, to SW-  
244 NE towards the limits of the seismic survey (Fig. 8b).

245 Channel Complex System 2 shows similar sinuosity to Channel Complex System 1, i.e. it is sinuous on  
246 the footwall and meandering on the hanging-wall (Figs. 8a and 8b). When compared to Channel Complex  
247 System 1, its vertical stacking becomes less marked near the Parihaka Fault (Fig. 6c). On the hanging-wall,  
248 the channel complex system becomes less confined towards the NE (Fig. 8b) where a maximum thickness of  
249 300 m is observed. Accommodation space was created during the reactivation of S2, as this fault segment is  
250 continuous on the seismic profiles flattened at horizon TC (Figs. 8c and 8d). The geometry of the relay ramp  
251 developed between segments S2 and S3 shows rotation of S2 in relation to the footwall and the hanging-wall  
252 blocks (Fig. 6c), with subsequent development of horsetail splays at its upper tip, offsetting Channel System  
253 2.

254

#### 255 *4.3. Channel Complex System 3*

256

257 Channel Complex System 3 is >15 km long and located in the northern part of the study area (Figs. 9a  
258 and 9b). The base of this channel complex system incises horizon TC close to segment S3 (Fig. 9a). It then  
259 migrates towards the NE, where it deepens to 1450 ms TWT (Fig. 9b). This channel system is characterised  
260 by two tributaries that form angles of 71° and 60° relative to the NNE-striking segment S3 (Fig. 9a).

261 Channel Complex System 3 is an example of a channel system transverse to S3 (Figs. 9a and 9b). Channel  
262 confluence occurs on the fault-bounded slope formed between the footwall and hanging-wall blocks, and  
263 Channel Complex System 3 becomes perpendicular to the Parihaka Fault towards the east, where it reaches its  
264 maximum thickness (300 m). In contrast to Channel Complex Systems 1 and 2, this channel system does not  
265 show a dramatic decrease in confinement close to depocentre 1.

266 A ~ 4 km width relay ramp comprising segments S2 and S3 of the Parihaka Fault is observed to the south  
267 of Channel Complex System 3 (see section E-F, Fig. 6c), whereas a ~ 500 m width relay ramp formed between  
268 segments S3 and S4 occurs to the north (see section G-H, Fig. 6d). Despite the occurrence of these two relay  
269 ramps, Channel Complex System 3 flows transversally to S3. Channel Complex System 3 is mostly sinuous,  
270 on both the footwall and hanging-wall blocks (Figs. 9a and 9b).

271 As Channel Complex System 3 incises horizon TC, and is thus younger than 2.5 Ma, we flattened the  
272 seismic profile in Fig. 9c using horizon H<sub>3</sub> (1.26 Ma) as reference. The flattening reveals a continuous S3, and  
273 suggests that the development and growth of this fault segment had an important role in the creation of  
274 accommodation space later filled by Channel Complex System 3 (Fig. 9d).

275

#### 276 *4.4. Channel Complex System 4*

277

278 Channel Complex System 4 is a >18 km long meandering channel complex system located in the northern  
279 part of the study area. It incises a prograding sequence on the footwall block (Fig. 10a). This channel complex  
280 system is not offset by any of the Parihaka Fault segments. However, at a distance of 2 km from S3, the erosive  
281 base of the channel changes from SW to NW, following a direction that is initially parallel to S3 to then trends  
282 53° to NW.

283 Channel System 4 remains mostly confined and reaches a maximum thickness of 300 m towards the end  
284 of the seismic survey (Fig. 10b). This conduit was filled in a series of multistorey nested offset to vertically  
285 stacked channel complex sets, before changing its course to NW (Figs. 6c and 10c).

286

287

### 288 **5. Channel density in the study area**

289 Channel Point (CP) distribution maps (Fig. 5b to 5e), and corresponding density plots (Fig. 11), reveal  
290 that channels occur predominantly between 864 ms and 1152 ms TWT on the footwall block (Figs. 5b and 11).  
291 Channel Points for Channel Complex System 4 are concentrated in the interval between 1152 ms and 1440 ms  
292 TWT (Fig. 5c). A large channel is observed in the southwestern portion of the study area at a depth ranging

293 from 1440 ms to 1728 ms TWT (Fig. 5d). Channel points on the hanging-wall block predominate at depths  
294 ranging from 1152 ms to 1440 ms TWT and 1440 ms to 1728 ms TWT (Figs. 5c and 5d). Only a small number  
295 of channels were recorded between 1728 ms and 2016 ms TWT (Fig. 5e).

296 Two areas of relatively high channel concentration are observed on density point data (Fig. 11). The first  
297 area corresponds to the position of Channel Complex System 4 on the footwall block. The second area is  
298 located adjacently to the hanging-wall of S2, in the position of Channel Complex System 2 (Fig. 11). Figure  
299 11 also shows a medium channel density in the areas corresponding to Channels Systems 1 and 3. Channel  
300 density is low adjacently to the three relay ramps developed between the Parihaka Fault segments (Fig. 11).

301

## 302 **6. Discussion**

### 303 *6.1. The Parihaka Fault and associated drainage systems*

304 In this work, two factors emerge as major controls on the creation of hanging-wall depocentres: 1) the  
305 reactivation of the Parihaka Fault segments S1 and S2, and the later development of S3 and S4, and 2) the high  
306 sedimentation rates recorded in the Taranaki Basin during the Plio-Pleistocene. These two controls are  
307 interpreted to have influenced channel evolution and distribution at different scales (Fig. 12). In the study area,  
308 three main drainage types related to the orientation of fault segments are observed: oblique, transverse, and  
309 parallel drainage (Fig. 12). The distribution, position and thickness of each of these drainage types were  
310 controlled by the orientation of the fault segments, fault displacement and tectonic subsidence rates (Eliet and  
311 Gwathorpe, 1995; Ge et al., 2017; Henstra et al., 2016; Morgan, 2004; Ravnås and Steel, 1998; Soreghan et  
312 al., 1999).

313 Channel Complex System 1 is an example of an oblique drainage system where its largest tributary,  
314 located in the southern part of the study area, forms an angle of 44° relative to S1 (Figs. 7a and 12). Two other  
315 tributaries of this channel system, forming angles of 65° and 71° relative to segment S1, are also identified on  
316 the footwall block (Fig. 7b). On the hanging-wall block, multistorey vertically and laterally nested channel  
317 complex sets are observed (Fig. 7c).

318 The flattened seismic section in Fig. 7d suggests that Channel Complex System 1 was initially developed  
319 in the southern part of the study area, before S1 was reactivated in the Early Pliocene. However, from Fig. 12  
320 one can also observe a clear relationship between the angles between tributaries in Channel Complex System  
321 1 and segment S1. Fault throw is also larger towards the centre of the fault, where channel tributaries converge,  
322 indicating that the reactivation of segment S1 affected the channels (Fig. 12) by creating accommodation space  
323 on the hanging-wall block (Fig. 4c).

324 Channel Complex System 2 is an example of a transverse drainage system showing deflection of its initial  
325 path towards the trace of segments S2 and S3 (Fig. 8). Deflections in Channel Complex System 2 reveal that  
326 channel evolution was controlled by fault orientation and uplift and rotation of the footwall block (Hubbard et  
327 al., 2014; Soreghan et al., 1999). The seismic profile flattened on horizon TC shows a continuous segment S2  
328 at 2.45 Ma, suggesting that it was active at this time and contributing to the creation of accommodation space  
329 on the hanging-wall block (Fig. 8d). It also indicates that downslope progradation of the Giant Foresets

330 Formation sediments, downstream of segments S1 and S2, occurred in at least two phases when considering  
331 Channel Complex Systems 1 and 2. The first phase (~4.5 Ma) is syn-tectonic and related to incision of the  
332 fault-bounded slope between the footwall and hanging-wall blocks, corresponding to the early stages of fault  
333 growth and subsidence of the Northern Graben (Giba et al., 2012). The second phase (~3 Ma) is related to a  
334 relative sea level lowstand and is characterised by sediment bypass towards the basin depocentre (Salazar et  
335 al., 2016). It deposited relatively less confined, thicker deposits (Figs. 8c and 8d).

336 Channel Complex System 3 is another example of a transverse drainage system. In contrast to Channel  
337 Complex System 2, this channel system incises horizon TC with two tributaries that converge on the slope of  
338 S3. Such a geometry indicates that the deposition of Channel Complex System 3 occurred during the Late  
339 Pliocene, whereas Channel Complex Systems 1 and 2 developed during the Early Pliocene. The geometry of  
340 Channel Complex System 3 highlights the active growth of segment S3 (Fig. 9).

341 Transverse channel migration was responsible for both lateral migration and vertical stacking of channels  
342 in the study area. The syn-tectonic evolution of Channel Complex Systems 2 and 3, due to reactivation of S2  
343 and onset of S3 is characteristic of half-graben systems showing transverse drainage systems, and common in  
344 areas of active extensional tectonics (Ge et al., 2017; Ravnås and Steel, 1998). An analogue example is  
345 observed in the Niger Delta, where half-grabens have continuously controlled the position and distribution of  
346 turbidite channel complexes in proximal areas of the Nigeria's continental slope (Morgan, 2004).

347 Channel Complex System 4 is located on the footwall block of the Parihaka Fault, with an initial SW-NE  
348 direction (Figs. 10a and 10b). Instead of following oblique to transverse pathways in relation to the fault trace,  
349 Channel Complex System 4 is deflected in the proximity of S3. The movement of S3 and S4 in the northern  
350 part of the study area resulted in the rotation and uplift of the footwall block close to the fault scarp. This is  
351 the main cause for the diversion of Channel Complex System 4 to the NW of the study area (Figs. 10a and  
352 10b).

353 Local subsidence along the Parihaka Fault is interpreted from the sediment thickness map extracted  
354 between horizons BC and TC, where two depocentres were developed on the hanging-wall block towards the  
355 NE (Fig. 4c). The generation of accommodation space in Depocentres 1 and 2, and the large volume of  
356 sediment accumulated on the hanging-wall block, indicate the Parihaka Fault controlled the distribution of  
357 sediments in the study area. Relative isolation of the footwall block and marked thickening of strata on the  
358 hanging-wall block are particularly observed along the Early Pliocene - Recent segments S3 and S4.

359 The sinuosity values observed for Channel Complex Systems 1 to 3 indicate that channels are more  
360 sinuous on the footwall block. On the hanging-wall block, channels vary from straight to meandering and show  
361 a complex geometry, with complex vertical and lateral stacking patterns in channel complex sets. Changes in  
362 the dip directions of channel incisions due to an increase in the slope (Deptuck et al., 2003; Gee and Gawthorpe,  
363 2006) are also observed. This occurs due to the levelling out of the hanging-wall slope as strata thickens  
364 (Gawthorpe and Leeder, 2000), favouring progradation in areas of high sediment supply.

365

366 *6.2. Limited influence of relay ramps on sediment sourcing into hanging-wall deposition*

367 Displacement accommodation between individual fault segments is often enhanced by the formation of  
368 intrabasin transfer zones or relay ramps, especially when the geometry of faults follows an en echelon stepping  
369 pattern (Leeder and Gawthorpe, 1987). Intrabasin relay ramps may influence sedimentation trends on a local  
370 scale to act as pathways for turbidity currents, especially in transverse drainage systems (Anderson et al., 2000;  
371 Athmer et al., 2010; Fugelli and Olsen, 2007; Gawthorpe and Hurst, 1993; Ravnås and Steel, 1998; Rotevatn  
372 et al., 2007; Young et al., 2001). A decrease in elevation towards the ramp is normally associated with  
373 intrabasin transfer zones (Gawthorpe and Hurst, 1993; Paul and Mitra, 2013). Individual transfer zone  
374 morphologies, however, are poorly constrained on subsurface data (Gawthorpe and Hurst, 1993; Gibbs, 1989).

375 The relay ramps developed between the Parihaka Fault segments are well-preserved in our seismic  
376 volume. Giba et al. (2012) examined the kinematic evolution of the relay zone developed between segments  
377 S1 and S2, which shows an overlap of 2.8 km. The transfer zone developed between segments S2 and S3 of  
378 the Parihaka Fault is fully breached and could act as a conduit for sediment flow onto the hanging wall. One  
379 could expect Channel Complex System 3 to follow this relay ramp. However, Channel Complex System flows  
380 transversally to S3 instead of flowing towards the relay ramp, forming a more abrupt sediment pathway  
381 towards the hanging-wall block. This likely occurred due to the effectiveness of the channel systems in  
382 containing sediment flow while incising the slope.

383 The geometry of relay ramps in the study area is consistent with the axial through-drainage facies model  
384 of Leeder and Gawthorpe (1987), in which mini-grabens developed in the zone between two *en echelon* normal  
385 faults confine the channel deposits as vertically-stacked units bounded by faults. However, the transverse  
386 orientation of the channels flowing towards the Parihaka Fault segments, the absence of interpreted submarine  
387 fans on the seismic profiles, and cross-correlations between channel-density (Fig. 11) and thickness data (Fig.  
388 4c), do not show a concentration of channels around the transfer zones to support the trapping of channel  
389 deposits by relay ramps.

390 A ~ 500 m width transfer zone developed between segments S3 and S4 was identified as an unbreached  
391 relay ramp, as these segments are not linked at depth (Fig. 6d). Its development resulted from the large  
392 displacement of the northern section of the fault system due to its sub-optimal strike in relation to regional  
393 extension. The large displacement recorded in the northern part of the study area led to repeated rotation of  
394 beds in the relay ramp, and significant hanging-wall deformation (Giba et al., 2012), a factor accounting for  
395 the lower gradient slope and offset in this zone. The submarine channels surrounding the ramp do not show a  
396 clear convergence of footwall drainage systems flowing through the relay ramp, preferentially feeding into the  
397 hanging wall sub-basin.

398

### 399 6.3. Channel deposit thickness and implications for petroleum systems

400 While significant subsidence occurred in the Taranaki Basin during the Cretaceous-Eocene (Giba et al.,  
401 2012; King and Thrasher, 1996), this study focuses on the Pliocene syn-rift phase, in which submarine channel  
402 complex systems were able to form. The thickness map of the main channel section (between horizons BC and  
403 TC; Fig. 4c) and seismic profiles in Figs. 7 to 10 indicate that the accommodation space was primarily located

404 on the hanging-wall block of the Parihaka Fault system, where two depocentres were formed to the NE of the  
405 study area (Fig. 4c). However, the great thickness of the hanging-wall block is not reflected in the channel  
406 density plot (Fig. 11), where channel density is shown to be larger around Channel Complex Systems 2 and 4.  
407 Evidence for channels close to relay ramps is scarce both on the channel density plot (Fig. 11) and on the  
408 isochron map in Fig. 4c. This latter observation proves the minor influence that relay ramps had on channel  
409 configuration (Fig. 11).

410 Fault activity in the Cape Egmont Fault Zone may have an important control on petroleum system in the  
411 North Taranaki Graben. The deposition of the Giant Foresets Formation during the Pliocene was synchronous  
412 with the growth of the Parihaka Fault and subsequent generation of accommodation space on the hanging-wall  
413 block, resulting in the formation of two depocentres in the NE. Vertically and laterally stacked channel deposits  
414 of Channel Complex Systems 2 and 3, on the hanging-wall of the Parihaka Fault, comprise a potential reservoir  
415 for hydrocarbons generated in the Moki Formation. As thick channel deposits are observed on the hanging-  
416 wall block, they will be important for the development of petroleum systems in the northern Taranaki Basin  
417 (Armstrong et al., 1996; Funnell et al., 1996; Hansen and Kamp, 2004b; Webster et al., 2011).

418 The rapid deposition of sediment in the Giant Foresets Formation can either influence the migration of  
419 hydrocarbons or comprise a potential hydrocarbon reservoir seal (Stagpoole and Funnell, 2001). Rapid  
420 sediment accumulation rates during basin development may also contribute to increasing thermal gradients,  
421 hydrocarbon maturation and migration through a petroleum system (Spencer, 1987). However, no evidence  
422 for fluid accumulations were found in the interpreted seismic data. The well Arawa-1 recorded three significant  
423 dry gas peaks at the top of the Moki Formation, below the interval of interest of this work (Arco, 1992). Based  
424 on the interactions between tectonic subsidence and fast sedimentation related to the opening of the Northern  
425 Graben we can infer any fluids generated in the study area migrated upwards along the Parihaka Fault.

426

## 427 7. Conclusions

428 The importance of structural controls on submarine channel deposits motivated the analysis of the  
429 Parihaka 3D seismic volume as a case study that can be extrapolated to other areas where faulting influences  
430 the geometry of channel drainage networks. In parallel, this study aimed at evaluating the location of large  
431 depocentres on the hanging-wall block of the Parihaka Fault, some with potential reservoir intervals. The main  
432 conclusions of this work can be summarised as follows:

- 433 a) The reactivation of segments S1 and S2 in the Parihaka Fault (Early Pliocene to Pleistocene) and the  
434 formation of segments S3 and S4 from 2.4 Ma until the present day, generated important accommodation  
435 space. This is demonstrated by the formation of two large depocentres on the hanging-wall block of the  
436 Parihaka Fault.
- 437 b) Transverse, oblique and parallel drainage types were developed relative to the Parihaka Fault. Channel  
438 Complex System 1, located in the southern part of the study area, is an example of a drainage system  
439 flowing obliquely to S1 during the reactivation of this segment. Channel Complex Systems 2 and 3 initially

440 flow obliquely to the Parihaka Fault and are later diverted transversally, incising segments S2 and S3.  
441 Channel Complex System 4 flows parallel to the fault trace on the footwall block due to footwall uplift  
442 associated with segments S3 and S4.

443 c) Relay Ramps were developed between distinct fault segments. However, submarine channels did not use  
444 the relay ramps as main pathways for the sediments. Channel Complex Systems 2 and 3, for instance,  
445 changed their original courses and flowed transversally relative to the Parihaka Fault trace, instead of  
446 flowing through the relay ramps.

447 d) Channel systems are concentrated on both the footwall and hanging-wall blocks of the Northern Graben,  
448 with two depocentres identified in the NE. We propose that Channel Complex System 2, on the footwall  
449 block, comprises an important hydrocarbon reservoir in the study area. Vertically- and laterally-stacked  
450 channel complex systems, where the progradational sequences of the Giant Foresets Formation rapidly  
451 accumulated on the hanging-wall block, may also comprise competent reservoir units in the study area.

## 452 **Acknowledgments**

453 The authors would like to acknowledge the New Zealand Petroleum Board for the use of data included in this paper. The  
454 first author would like to acknowledge CAPES (Coordenação de Aperfeiçoamento de Pessoal de Nível Superior – Brazil)  
455 for the PhD grant no. 99999.000877/2014-00. Schlumberger is acknowledged for the provision of the academic licences  
456 of Petrel® to Cardiff University 3D Seismic Lab. We thank Editor Atle Rotevatn, Migdalys Salazar, Larissa Hansen and  
457 Clark Gilbert for their constructive comments on this manuscript.

## 458 **References**

459 Abreu, V., Sullivan, M., Pirmez, C., & Mohrig, D. 2003. Lateral accretion packages (LAPs): an important reservoir element  
460 in deep water sinuous channels. *Marine and Petroleum Geology*, 20(6-8), 631-648.

461 Anderson, J.E., Cartwright, J., Drysdall, S.J., Vivian, N., 2000. Controls on turbidite sand deposition during gravity-driven  
462 extension of a passive margin: examples from Miocene sediments in Block 4, Angola. *Marine and Petroleum Geology*,  
463 17, 1165-1203.

464 Arco Petroleum, 1992. Arawa-1 Final Well Report PPL 38436, in Ministry of Economic Development, New Zealand:  
465 Crown Minerals Unpublished Petroleum Report, PR 1824.

466 Armstrong, P.A., Chapman, D.S., Funnell, R.H., Allis, R.G., Kamp, P.J., 1996. Thermal modeling and hydrocarbon  
467 generation in an active-margin basin: Taranaki Basin, New Zealand. *AAPG Bulletin* 80, 1216-1241.

468 Athmer, W., Groenenberg, R.M., Luthi, S.M., Donselaar, M.E., Sokoutis, D., & Willingshofer, E. 2010. Relay ramps as  
469 pathways for turbidity currents: a study combining analogue sandbox experiments and numerical flow simulations.  
470 *Sedimentology*, 57(3), 806-823.

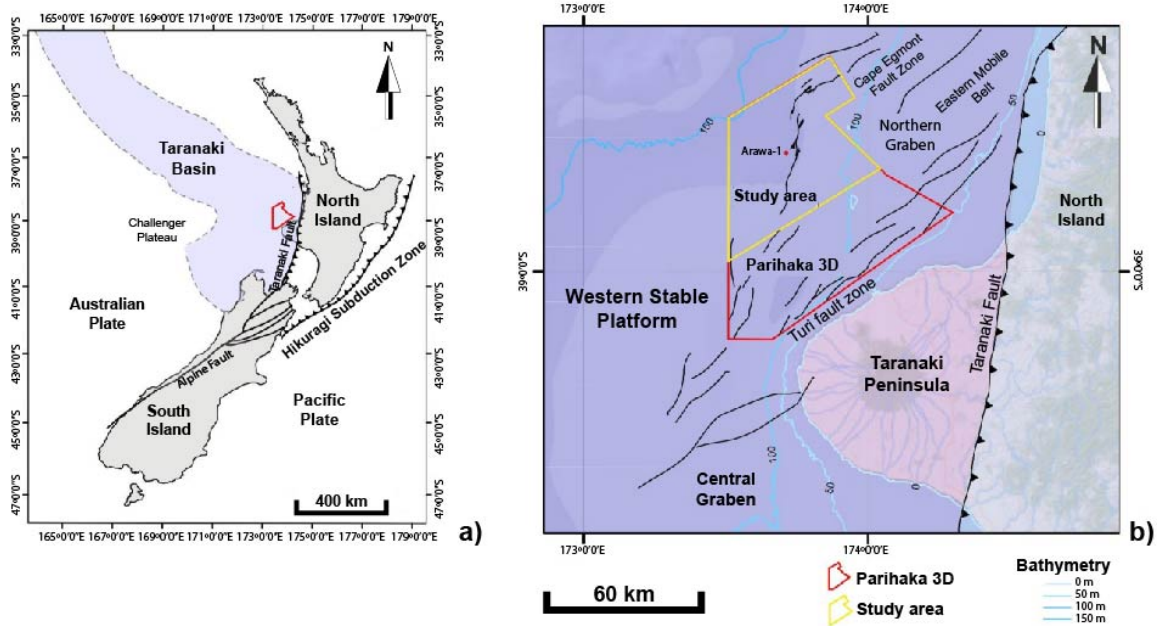
471 Athmer, W., Luthi, S.M., 2011. The effect of relay ramps on sediment routes and deposition: A review. *Sedimentary*  
472 *Geology* 242, 1-17.

- 473 Childs, C., Manzocchi, T., Walsh, J. J., Bonson, C. G., Nicol, A., & Schöpfer, M. P. 2009. A geometric model of fault zone  
474 and fault rock thickness variations. *Journal of Structural Geology*, 31(2), 117-127.
- 475 Clark, J. D., & Pickering, K. T. 1996. Architectural elements and growth patterns of submarine channels: application to  
476 hydrocarbon exploration. *AAPG Bulletin*, 80(2), 194-220.
- 477 Crundwell, M.P.; Beu, A.G.; Morgans, H.E.G.; Mildenhall, D.C.; Wilson, G.S. 2004: Chapter 12, Miocene. In Cooper,  
478 R.A. (ed.) 2004. The New Zealand Geological Timescale. Institute of Geological and Nuclear Sciences Monograph 22.  
479 284 p.
- 480 Deptuck, M. E., Steffens, G. S., Barton, M., & Pirmez, C. 2003. Architecture and evolution of upper fan channel-belts on  
481 the Nger Delta slope and in the Arabian Sea. *Marine and Petroleum Geology*, 20(6), 649-676.
- 482 Eliet, P. P., & Gawthorpe, R. L. 1995. Drainage development and sediment supply within rifts, examples from the Sperchios  
483 basin, central Greece. *Journal of the Geological Society*, 152(5), 883-893.
- 484 Fossen, H., & Rotevatn, A. 2016. Fault linkage and relay structures in extensional settings—A review. *Earth-Science*  
485 *Reviews*, 154, 14-28.
- 486 Fugelli, E.M., Olsen, T.R. 2007. Delineating confined slope turbidite systems offshore mid-Norway: The Cretaceous deep-  
487 marine Lysing Formation. *AAPG Bulletin*, 91(11), 1577-1601.
- 488 Funnell, R., Chapman, D., Allis, R., Armstrong, P., 1996. Thermal state of the Taranaki basin, New Zealand. *Journal of*  
489 *Geophysical Research: Solid Earth* (1978–2012) 101, 25197-25215.
- 490 Gamboa, D., Alves, T.M., Cartwright, J., 2012. A submarine channel confluence classification for topographically confined  
491 slopes. *Marine and Petroleum Geology*, 35, 176-189.
- 492 Gawthorpe, R.L., Fraser, A.J., Collier, R.E.L. 1994. Sequence stratigraphy in active extensional basins: implications for  
493 the interpretation of ancient basin-fills. *Marine and Petroleum Geology*, 11(6), 642-658.
- 494 Gawthorpe, R.L., Hurst, J., 1993. Transfer zones in extensional basins: their structural style and influence on drainage  
495 development and stratigraphy. *Journal of the Geological Society*, 150, 1137-1152.
- 496 Gawthorpe, R.L., Leeder, M.R. 2000. Tectono-sedimentary evolution of active extensional basins. *Basin Research*, 12(3-  
497 4), 195-218.
- 498 Ge, Z., Nemeč, W., Gawthorpe, R. L., & Hansen, E. W. 2017. Response of unconfined turbidity current to normal-fault  
499 topography. *Sedimentology*, 64(4), 932-959.
- 500 Ge, Z., Nemeč, W., Gawthorpe, R. L., Rotevatn, A., & Hansen, E. W. 2018. Response of unconfined turbidity current to  
501 relay-ramp topography: insights from process-based numerical modelling. *Basin Research*, 30(2), 321-343.
- 502 Gee, M., Gawthorpe, R., 2006. Submarine channels controlled by salt tectonics: Examples from 3D seismic data offshore  
503 Angola. *Marine and Petroleum Geology* 23, 443-458.
- 504 Gee, M., Gawthorpe, R., Bakke, K., Friedmann, S., 2007. Seismic geomorphology and evolution of submarine channels  
505 from the Angolan continental margin. *Journal of Sedimentary Research* 77, 433-446.

- 506 Giba, M., Nicol, A., Walsh, J., 2010. Evolution of faulting and volcanism in a back-arc basin and its implications for  
507 subduction processes. *Tectonics* 29.
- 508 Giba, M., Walsh, J.J., Nicol, A., 2012. Segmentation and growth of an obliquely reactivated normal fault. *Journal of*  
509 *Structural Geology* 39, 253-267.
- 510 Gibbs, A.D. 1989. Structural styles in basin formation. In: Extensional Tectonics and Stratigraphy of the North Atlantic  
511 Margins. *AAPG Memoir*. Vol. 46, pp. 81-94.
- 512 Gupta, S., Underhill, J., Sharp, I., Gawthorpe, R., 1999. Role of fault interactions in controlling synrift sediment dispersal  
513 patterns: Miocene, Abu Alaqa Group, Suez Rift, Sinai, Egypt. *Basin Research* 11, 167-189.
- 514 Hansen, R.J., Kamp, P.J., 2002. Evolution of the Giant Foresets Formation, northern Taranaki Basin, New Zealand.
- 515 Hansen, R.J., Kamp, P.J., 2004a. Late Miocene to early Pliocene stratigraphic record in northern Taranaki Basin: condensed  
516 sedimentation ahead of Northern Graben extension and progradation of the modern continental margin. *New Zealand*  
517 *journal of geology and geophysics* 47, 645-662.
- 518 Hansen, R.J., Kamp, P.J., 2004b. Rapid progradation of the Pliocene-Pleistocene continental margin, northern Taranaki  
519 Basin, New Zealand, and implications, Proceedings of New Zealand Petroleum Conference, pp. 7-10.
- 520 Henstra, G. A., Gawthorpe, R. L., Helland-Hansen, W., Ravnås, R., & Rotevatn, A. 2016. Depositional systems in  
521 multiphase rifts: seismic case study from the Lofoten margin, Norway. *Basin Research*. doi: 10.1111/bre.12183
- 522 Holt, W., Stern, T., 1991. Sediment loading on the western platform of the New Zealand continent: Implications for the  
523 strength of a continental margin. *Earth and planetary science letters* 107, 523-538.
- 524 Holt, W., Stern, T., 1994. Subduction, platform subsidence, and foreland thrust loading: The late Tertiary development of  
525 Taranaki Basin, New Zealand. *Tectonics* 13, 1068-1092.
- 526 Hopkins, M.C., Dawers, N.H. 2018. The role of fault length, overlap and spacing in controlling extensional relay ramp  
527 fluvial system geometry. *Basin Research*, 30(1), 20-34.
- 528 Hubbard, S.M., Covault, J.A., Fildani, A. and Romans, B.W., 2014. Sediment transfer and deposition in slope channels:  
529 deciphering the record of enigmatic deep-sea processes from outcrop. *Bulletin*, vol. 126, no. 5-6, pp.857-871.
- 530 Kamp, P.J., Vonk, A.J., Bland, K.J., Hansen, R.J., Hendy, A.J., McIntyre, A.P., Ngatai, M., Cartwright, S.J., Hayton, S.,  
531 Nelson, C.S., 2004a. Neogene stratigraphic architecture and tectonic evolution of Wanganui, King Country, and eastern  
532 Taranaki Basins, New Zealand. *New Zealand Journal of Geology and Geophysics* 47, 625-644.
- 533 Kamp, P.J., Vonk, A.J., Nelson, C.S., Hansen, R.J., Tripathi, A.R.P., Hood, S.D., Nagati, M., Hendy, A.J., 2004b.  
534 Constraints on the evolution of Taranaki Fault from thermochronology and basin analysis: Implications for the Taranaki  
535 Fault play.
- 536 King, P.R., 2000. Tectonic reconstructions of New Zealand: 40 Ma to the present. *New Zealand Journal of Geology and*  
537 *Geophysics* 43, 611-638.

- 538 King, P.R., Thrasher, G.P., 1996. Cretaceous Cenozoic geology and petroleum systems of the Taranaki Basin, New  
539 Zealand. Institute of Geological & Nuclear Sciences.
- 540 Lee, R. F. 2001. Pitfalls in seismic data flattening. *The Leading Edge*, 20(2), 160-164.
- 541 Leeder, M., Gawthorpe, R., 1987. Sedimentary models for extensional tilt-block/half-graben basins. *Geological Society,*  
542 *London, Special Publications* 28, 139-152.
- 543 Lomask, J. 2003. Flattening 3-D data cubes in complex geology. Stanford Exploration Project, Report, 113, 247-261.
- 544 Long, J. J., Imber, J. 2011. Geological controls on fault relay zone scaling. *Journal of Structural Geology*, 33(12), 1790-  
545 1800.
- 546 Mayall, M., Jones, E., & Casey, M. 2006. Turbidite channel reservoirs—Key elements in facies prediction and effective  
547 development. *Marine and Petroleum Geology*, 23(8), 821-841.
- 548 Morgan, R. (2004). Structural controls on the positioning of submarine channels on the lower slopes of the Niger Delta.  
549 *Geological Society, London, Memoirs*, 29(1), 45-52.
- 550 Morgans, H. E. G. 2006. Foraminiferal Biostratigraphy of the Early Miocene to Pleistocene Sequences in Witiara-1,  
551 Taimana-1, Arawa-1 and Okoki-1. GNS Science.
- 552 Mulrooney, M. J., Rismyhr, B., Yenwongfai, H. D., Leutscher, J., Olaussen, S., & Braathen, A. 2018. Impacts of small-  
553 scale faults on continental to coastal plain deposition: Evidence from the Realgrunnen Subgroup in the Goliat field,  
554 southwest Barents Sea, Norway. *Marine and Petroleum Geology*, 95, 276-302.
- 555 Neall, V., Stewart, R., Smith, I., 1986. History and petrology of the Taranaki volcanoes. *Royal Society of New Zealand*  
556 *Bulletin* 23, 251-263.
- 557 Nicol, A., Stagpoole, V., Maslen, G., 2004. Structure and petroleum potential of the Taranaki fault play, New Zealand  
558 Petroleum Conference Proceedings, pp. 7-10.
- 559 Nicol, A., Walsh, J., Berryman, K., Nodder, S., 2005. Growth of a normal fault by the accumulation of slip over millions  
560 of years. *Journal of Structural Geology* 27, 327-342.
- 561 Nodder, S.D., 1993. Neotectonics of the offshore Cape Egmont Fault Zone, Taranaki Basin, New Zealand. *New Zealand*  
562 *journal of geology and geophysics* 36, 167-184.
- 563 Paul, D., Mitra, S. 2013. Experimental models of transfer zones in rift systems. *AAPG bulletin*, 97(5), 759-780.
- 564 Peacock, D. C. P., Knipe, R. J., & Sanderson, D. J. 2000. Glossary of normal faults. *Journal of Structural Geology*, 22(3),  
565 291-305.
- 566 Peacock, D. C. P., & Sanderson, D. J. 1991. Displacements, segment linkage and relay ramps in normal fault zones. *Journal*  
567 *of Structural Geology*, 13(6), 721-733.
- 568 Pindell, J.L., 1995. Circum-Caribbean sedimentary basin development and timing of hydrocarbon maturation as a function  
569 of Caribbean plate tectonic evolution.

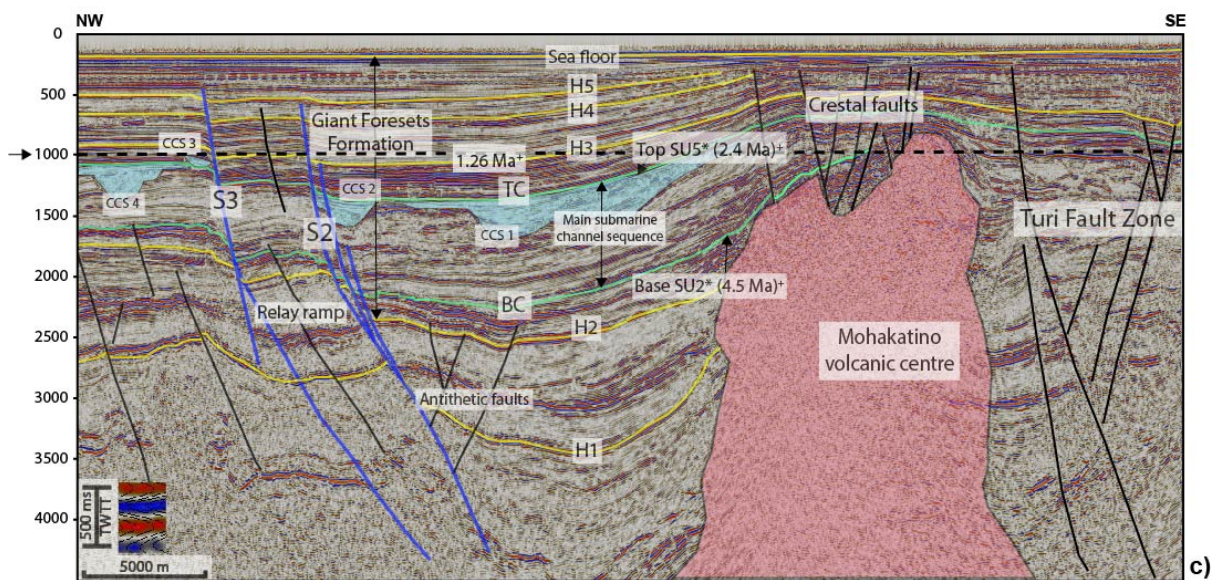
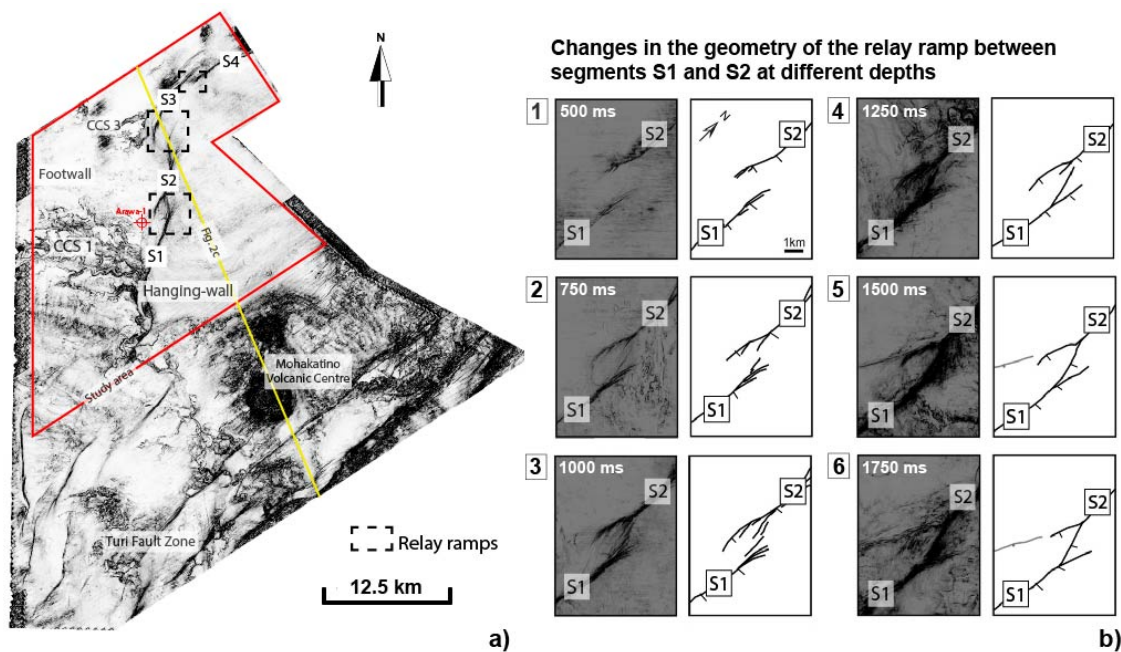
- 570 Posamentier, H. W., & Kolla, V. 2003. Seismic geomorphology and stratigraphy of depositional elements in deep-water  
571 settings. *Journal of sedimentary research*, 73(3), 367-388.
- 572 Ravnås, R., & Steel, R. J. 1998. Architecture of marine rift-basin successions. *AAPG Bulletin*, 82(8), 1626-1626.
- 573 Rotevatn, A., Fossen, H., Hesthammer, J., Aas, T.E., Howell, J.A. 2007. Are relay ramps conduits for fluid flow? Structural  
574 analysis of a relay ramp in Arches National Park, Utah. *Geological Society, London, Special Publications*, 270(1), 55-  
575 71.
- 576 Salazar, M., Moscardelli, L., Wood, L., 2016. Utilising clinoform architecture to understand the drivers of basin margin  
577 evolution: a case study in the Taranaki Basin, New Zealand. *Basin Research* 28, 840-865.
- 578 Soreghan, M. J., Scholz, C. A., & Wells, J. T. 1999. Coarse-grained, deep-water sedimentation along a border fault margin  
579 of Lake Malawi, Africa; seismic stratigraphic analysis. *Journal of Sedimentary Research*, 69(4), 832-846.
- 580 Spencer, C.W., 1987. Hydrocarbon generation as a mechanism for overpressuring in Rocky Mountain region. *AAPG*  
581 *Bulletin* 71, 368-388.
- 582 Stagpoole, V., Funnell, R., 2001. Arc magmatism and hydrocarbon generation in the northern Taranaki Basin, New  
583 Zealand. *Petroleum Geoscience* 7, 255-267.
- 584 Stagpoole, V., Nicol, A., 2008. Regional structure and kinematic history of a large subduction back thrust: Taranaki Fault,  
585 New Zealand. *Journal of Geophysical Research: Solid Earth* 113, n/a-n/a.
- 586 Walsh, J., Bailey, W., Childs, C., Nicol, A., Bonson, C., 2003. Formation of segmented normal faults: a 3-D perspective.  
587 *Journal of Structural Geology* 25, 1251-1262.
- 588 Webster, M., O'Connor, S., Pindar, B., Swarbrick, R., 2011. Overpressures in the Taranaki Basin: Distribution, causes, and  
589 implications for exploration. *AAPG Bulletin* 95, 339-370.
- 590 Young, M.J., Gawthorpe, R.L., Hardy, S. 2001. Growth and linkage of a segmented normal fault zone; the Late Jurassic  
591 Murchison–Statfjord North Fault, northern North Sea. *Journal of Structural Geology*, 23(12), 1933-195.
- 592



593

594 Figure 1: a) Regional location map of New Zealand and its main structural boundaries. The Taranaki Basin is limited to  
 595 the east by the Taranaki Fault and to the west by the Challenger Plateau. To the south, the Taranaki Basin is limited by  
 596 the South Island. The 3D seismic cube is delimited by the red polygon. b) Detailed location map of the Northern Graben  
 597 showing the main structures at a local scale. The study area occurs between 100 and 150 m below the sea level. The 705  
 598 km<sup>2</sup> study area is delimited by the yellow polygon.

599



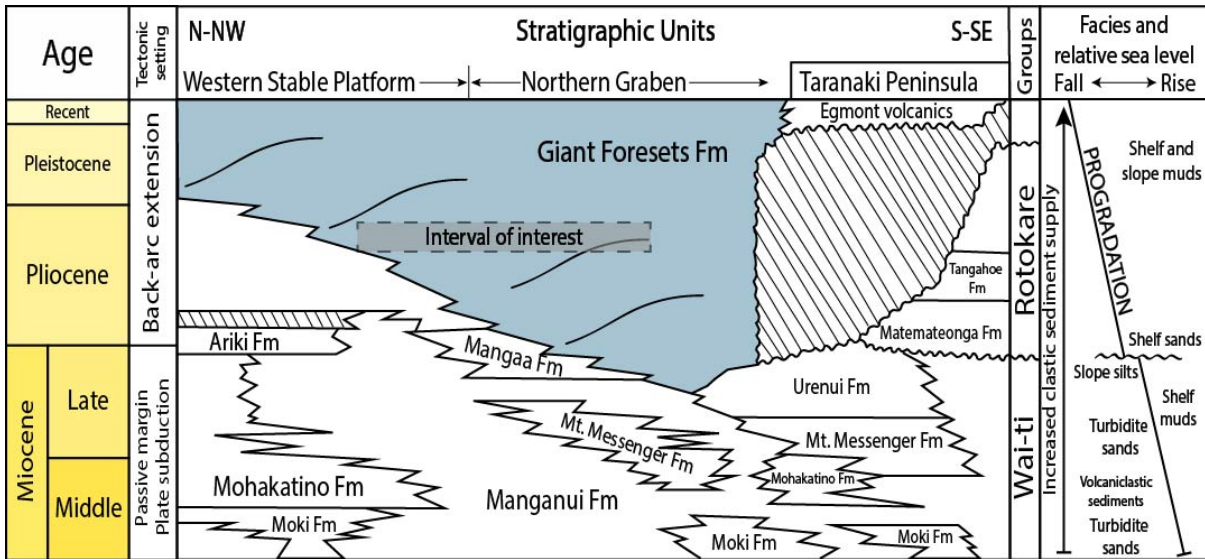
600

601

602 Figure 2: a) Variance slice at -1000 ms TWT showing main structural features in the interpreted seismic volume. The 705  
 603 km study area is delimited by the red polygon. b) Evolution of the relay ramp in the Parihaka Fault at each -250 ms TWT  
 604 showing the hard linkage of faults with depth. Unbreached relay ramp occur at shallow levels, as shown by the soft  
 605 linkage of the segments (Modified after Giba et al., 2012). c) Regional seismic profile showing the relay ramp developed  
 606 between segments S3 and S2 and main channel systems in the study area. The Mohakatino Volcanic Centre is observed  
 607 to the SE of the seismic line. The main submarine channel sequence is delimited by the horizons traced in green. CCS:  
 608 channel complex systems. \*Correlative seismic units from Salazar et al. (2016). Correlative ages from Morgans et al.  
 609 (2006). The location of this profile is indicated in Fig. 2a

610

611



612

613 Figure 3: Chronostratigraphic column showing depositional facies and relative sea-level changes in the Taranaki Basin  
 614 from the Miocene to the Recent. The interval of interest within the Giant Foresets Formation is highlighted in this figure.  
 615 Modified from King and Thrasher (1996).

616

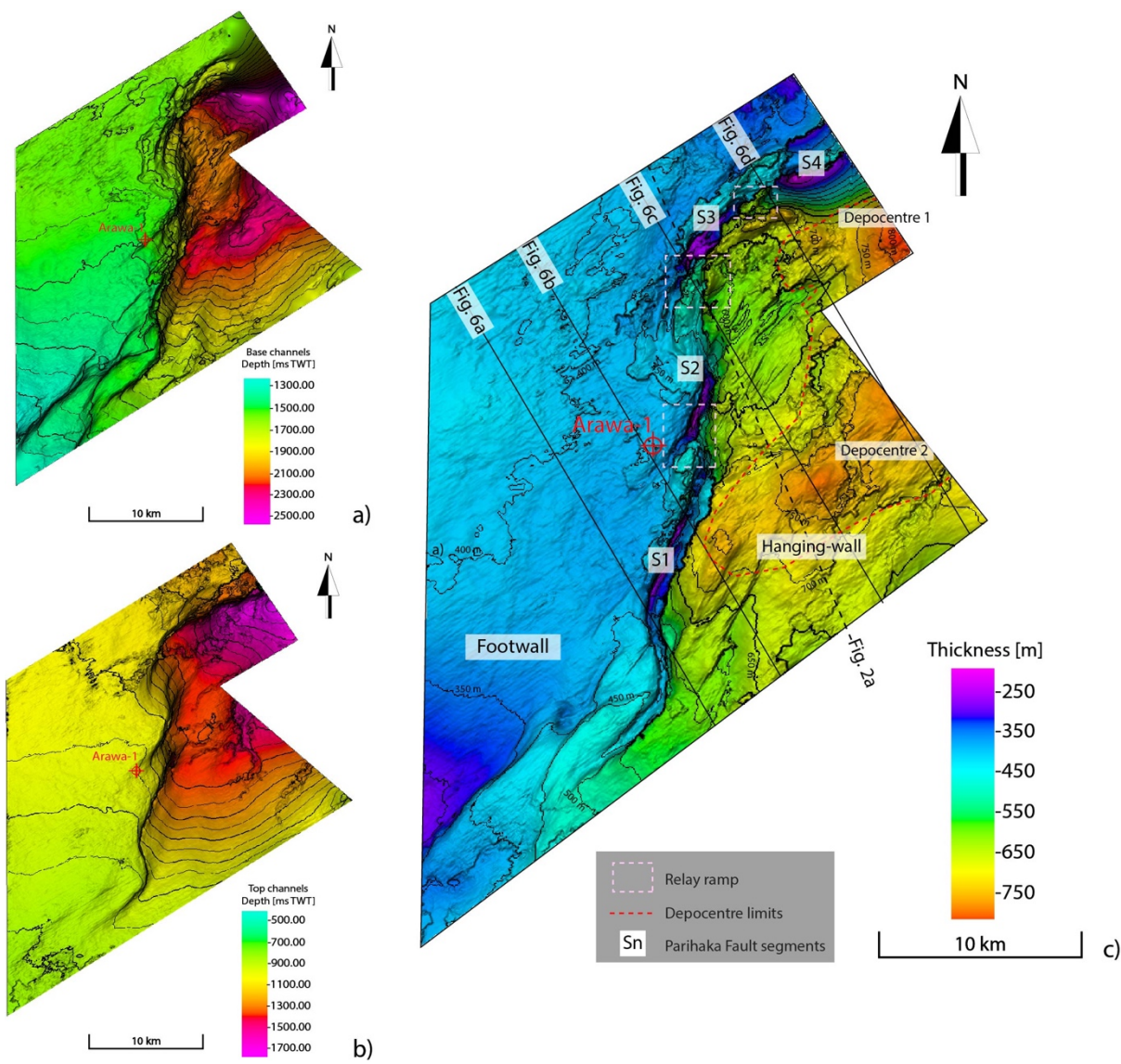
617

618

619

620

621

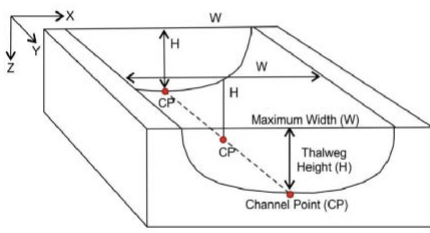


622

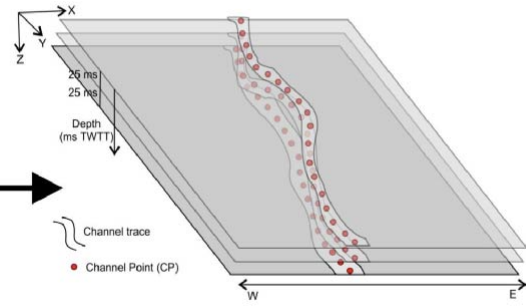
623 Figure 4: a) Time structure map for the Base Channel (horizon BC), highlighting the great depth in ms TWT difference  
 624 between the footwall (1250 to 1500 ms TWT) and the hanging-wall blocks (1500 to 2250 ms TWT) of the Parihaka Fault.  
 625 b) Time structure map for the Top Channel (horizon TC), indicating the depth (in ms TWT) differences between the  
 626 footwall (900 to 1050 ms TWT) and the hanging-wall (950 to 1450 ms TWT) are smaller than for horizon BC. The  
 627 interval of the contour lines is 50 ms. c) Isochron map for the between horizons BC and TC. The predominant thickness  
 628 for the footwall block is 400 m, whereas the thickness for the hanging-wall block ranges from 500 to 800 m. The interval  
 629 for the contour lines is 50 m. Depocentres 1 and 2 are delimited by the red dashed line and comprise the thickest deposits  
 630 in the study area.

631

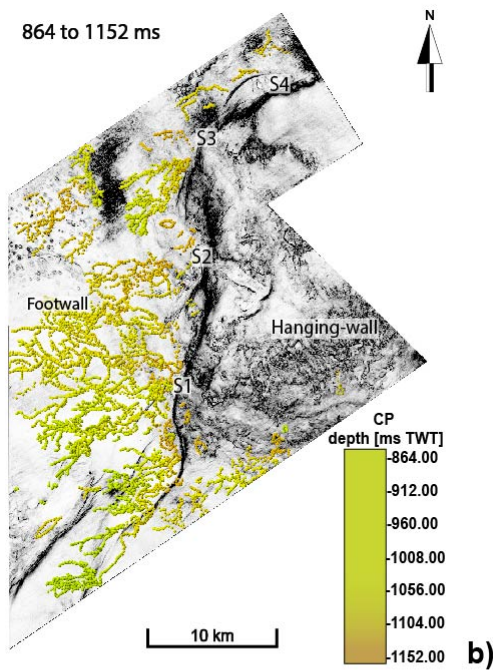
Measured parameters in single channel



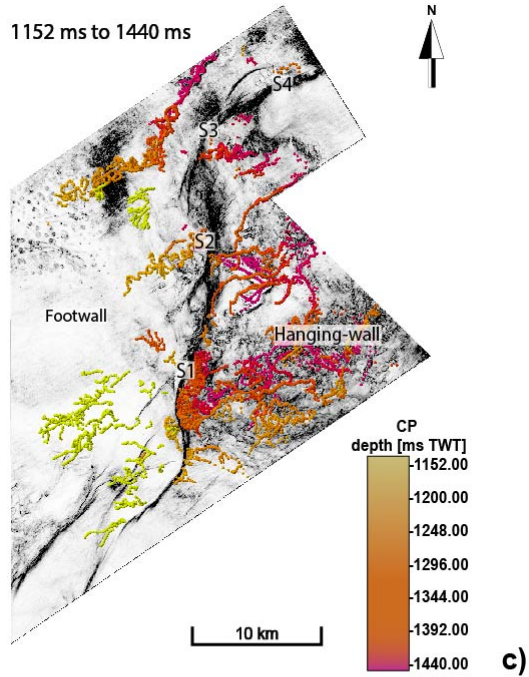
Method applied to channel features in consecutive variance time-slices



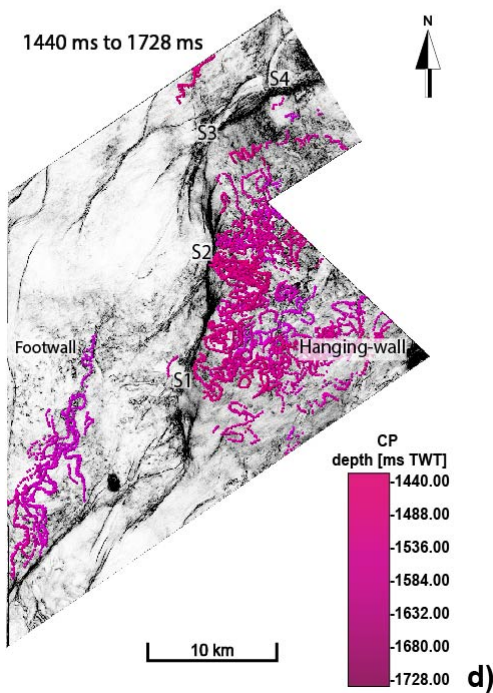
a)



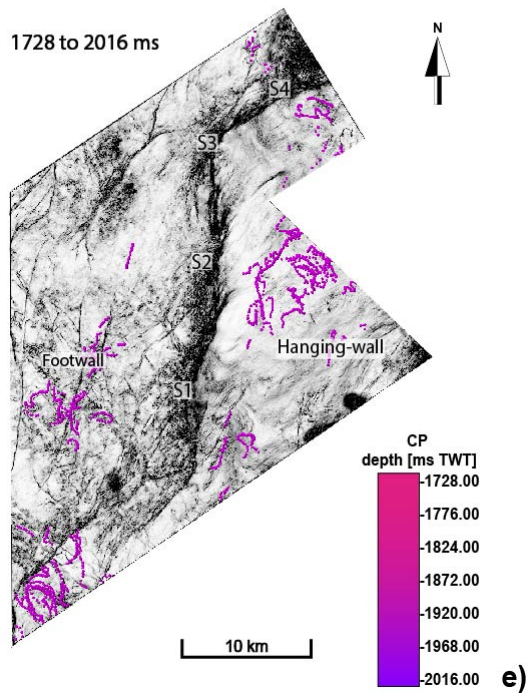
b)



c)



d)

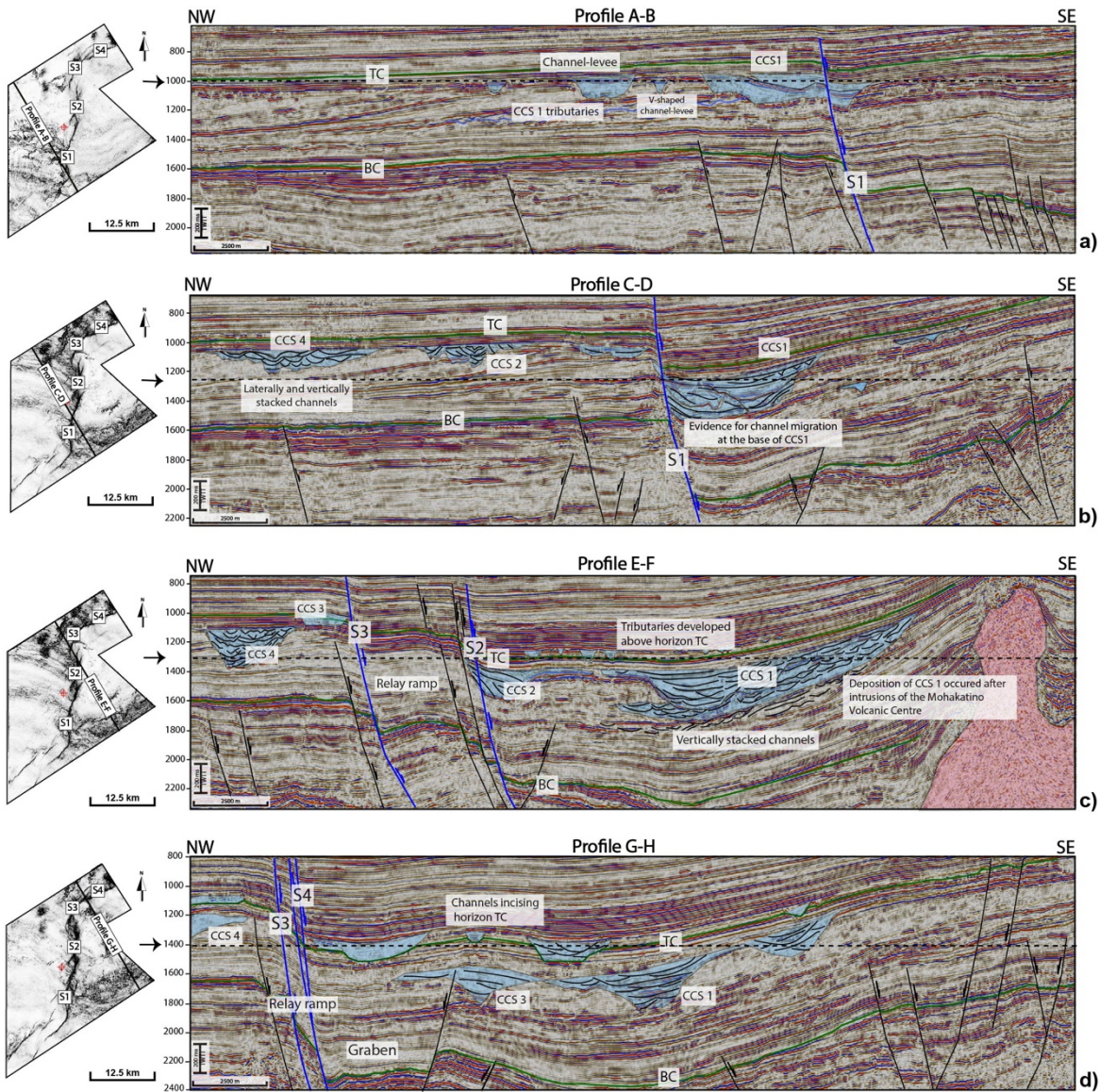


e)

633 Figure 5: Schematic representation of the morphometric analysis undertaken in this work. Height and width for channel  
 634 complex systems were measured from a reference Channel Point (CP) at the base of the variance time-slices. Modified  
 635 from Gamboa et al. (2012). Channel point distribution maps at depths from b) 864 to 1152 ms TWT, c) 1152 to 1440 ms  
 636 TWT, d) 1440 to 1728 ms TWT, and e) 1728 to 2016 ms TWT. These maps show channels predominate on the footwall  
 637 block between 864 and 1152 ms TWT. However, channel complex systems on the footwall block may occur at greater  
 638 depth. Channels on the hanging-wall block predominate between 1152 to 1728 ms TWT. Channel density is smaller from  
 639 1728 to 2016 ms TWT on both in the footwall and hanging-wall blocks of the Parihaka Fault.

640

641



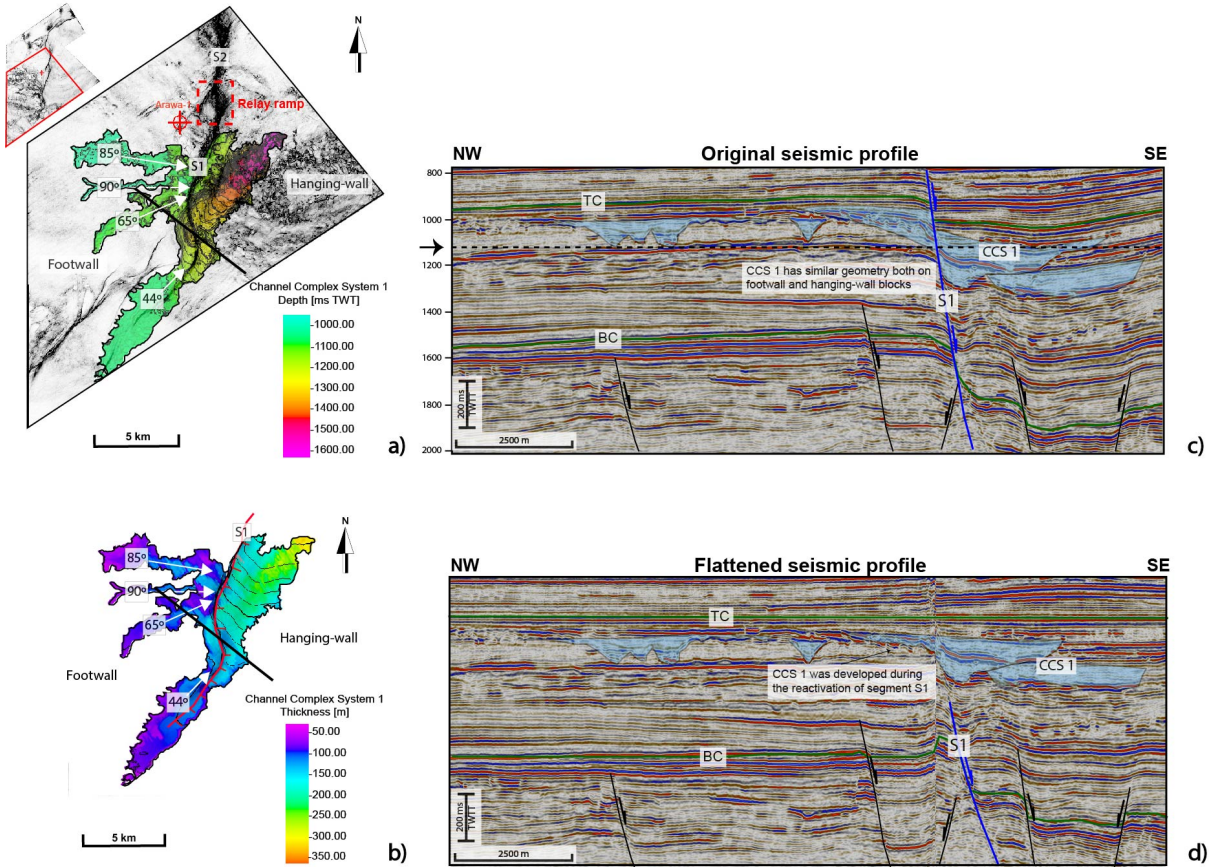
642

643 Figure 6: NW-SE seismic profiles of the study area highlighting the relationship between channel complex systems (CCS)  
 644 and the Parihaka Fault segments. a) Profile A-B shows the tributaries of Channel Complex System 1 to the NW consisting  
 645 of U and V-shaped erosional bases. Channel Complex System 1 occurs in the SE part of the seismic profile and is offset  
 646 by segment S1. b) Profile C-D show three of the four main channel systems in the study area. Channel Complex System  
 647 4 occurs to the NW on the footwall block and shows laterally and vertically stacked channels. Channel Complex System  
 648 2 occurs close to the trace of segment S1 and comprises two tributaries. Channel Complex System 1 occurs entirely on  
 649 the hanging-wall block in this profile and reveals the lateral and vertical stacking within this channel system. c) Profile  
 650 E-F shows Channel Complex System 4 system at a greater depth comprising many vertically stacked channels on the  
 651 footwall block. Channel Complex System 3 also occurs on the footwall block above Horizon TC and close to S3. A  
 652 rotated relay ramp developed between S3 and S2 is observed. Channel Complex System 2 is offset by S2 at the SE  
 653 termination of this relay ramp. Channel Complex System 1 occur at observed depths in the seismic survey between 1600  
 654 and 1800 ms TWT to the SE. d) Profile G-H shows a relay ramp developed between S3 and S4 in the NE part of the study

655 area. Channels developed above horizon TC are also observed on the hanging-wall block. The depths of time slices in  
656 insets are indicated by an arrow and a dashed line on the seismic profiles.

657

658



659

660 Figure 7: Detailed seismic interpretation of Channel Complex System 1 (CCS 1 in the figure boxes). a) Variance time-  
661 slice at 1180 ms showing the base of Channel Complex System 1 on the footwall block, the segments of Parihaka Fault,  
662 the position of the seismic section (yellow line), and the angles this channel system make in relation to S1. b) Thickness  
663 map for Channel System 1 showing the channel tributaries flowing obliquely to S1. c) Original seismic profile  
664 highlighting the channel geometry relative to the Parihaka Fault. The depth of the variance time-slice is indicated by an  
665 arrow and a dashed line on the seismic section. d) Seismic profile flattened at horizon TC highlighting the influence of  
666 faulting on channel configuration.

667

668

669

670

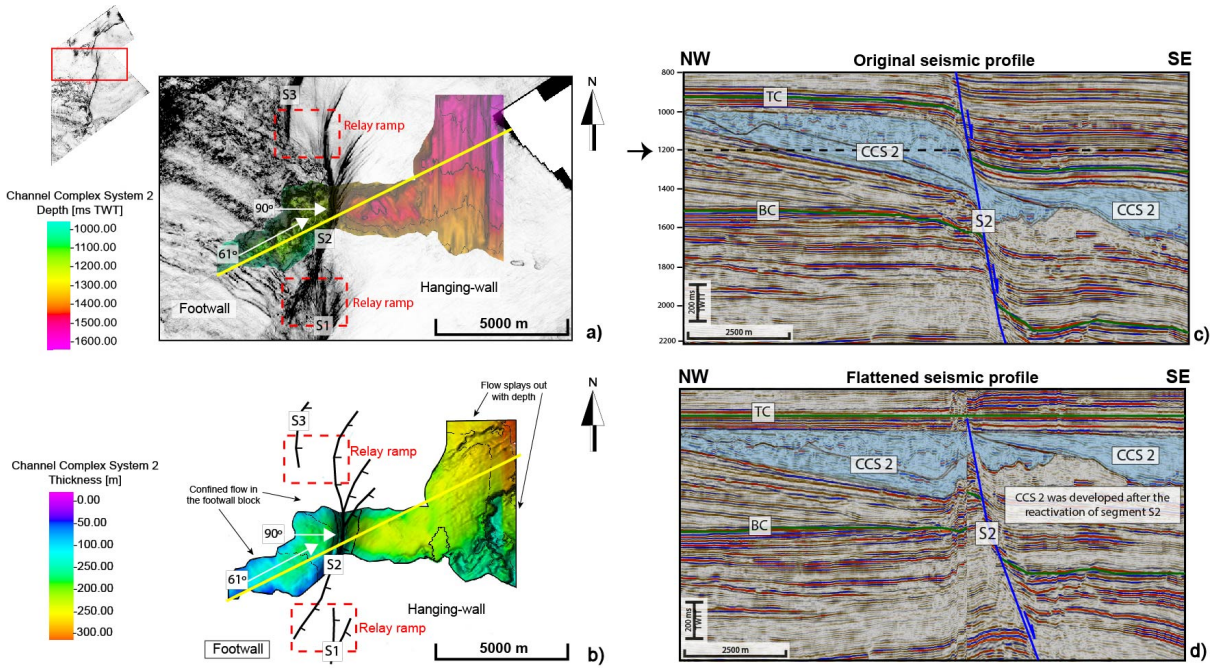
671

672

673

674

675



676

677 Figure 8: Detailed seismic interpretation of Channel Complex System 2 (CCS 2 in the boxes). a) Variance time-slice at a  
678 depth of 1200 ms TWT indicating the base of Channel Complex System 2 on the footwall block, the segments of Parihaka  
679 Fault, the position of the seismic section (yellow line), and the angles this channel system make to S2. b) Thickness map  
680 for Channel Complex System 2 showing the channel initially flowing obliquely to S2 to later change to a direction  
681 transverse to the segment trace. c) Original seismic profile highlighting the channel geometry relative to the Parihaka  
682 Fault. The depth of the variance time-slice is indicated by an arrow and a dashed line on the seismic profile. d) Flattened  
683 seismic profile at horizon TC showing the syn-tectonic deposition of Channel Complex System 2 during the reactivation  
684 of S2.

685

686

687

688

689

690

691

692

693

694

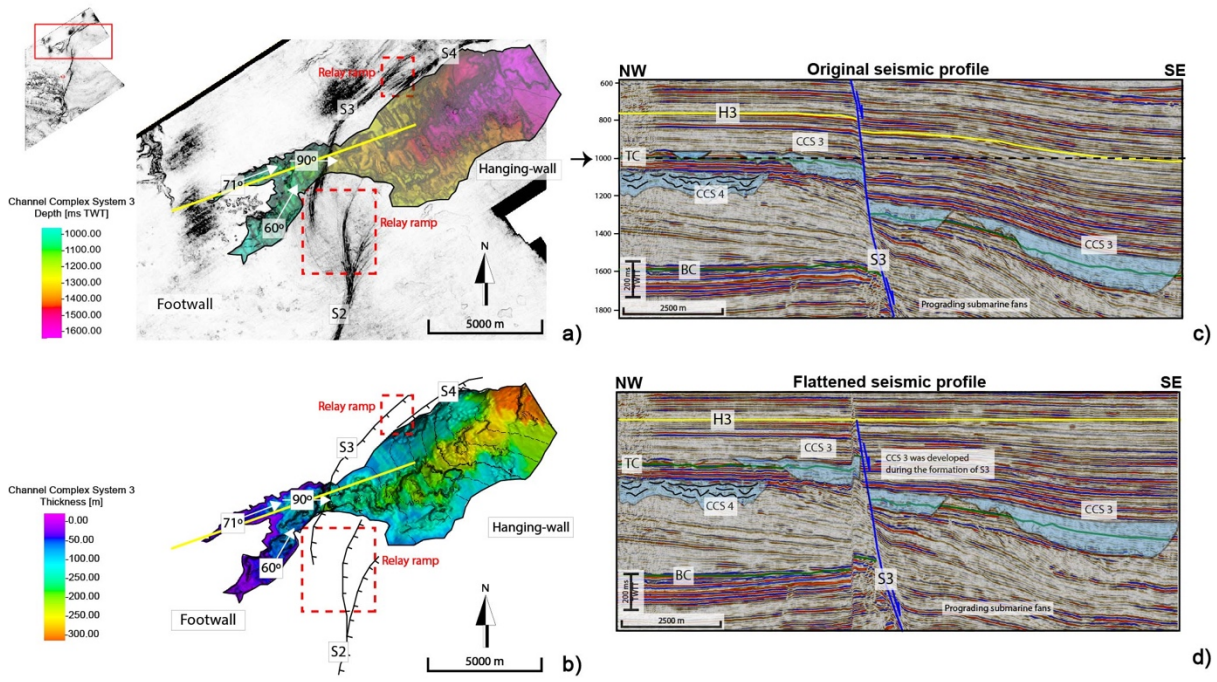
695

696

697

698

699



700

701 Figure 9: Detailed seismic interpretation of Channel Complex System 3 (CCS 3 in the boxes). a) Variance time-slice at  
 702 1020 ms indicating the base of Channel Complex System 3 on the footwall block, the segments of Parihaka Fault, the  
 703 position of the seismic profile (yellow line), and the angles this channel system make to S3. b) Thickness map for  
 704 Channel Complex System 3 showing the two main channel tributaries flowing obliquely to segment S3. c) Original  
 705 seismic profile highlighting the channel geometry relative to the Parihaka Fault. d) Flattened seismic profile at horizon  
 706 H3 highlighting faulting prior to channel deposition.

707

708

709

710

711

712

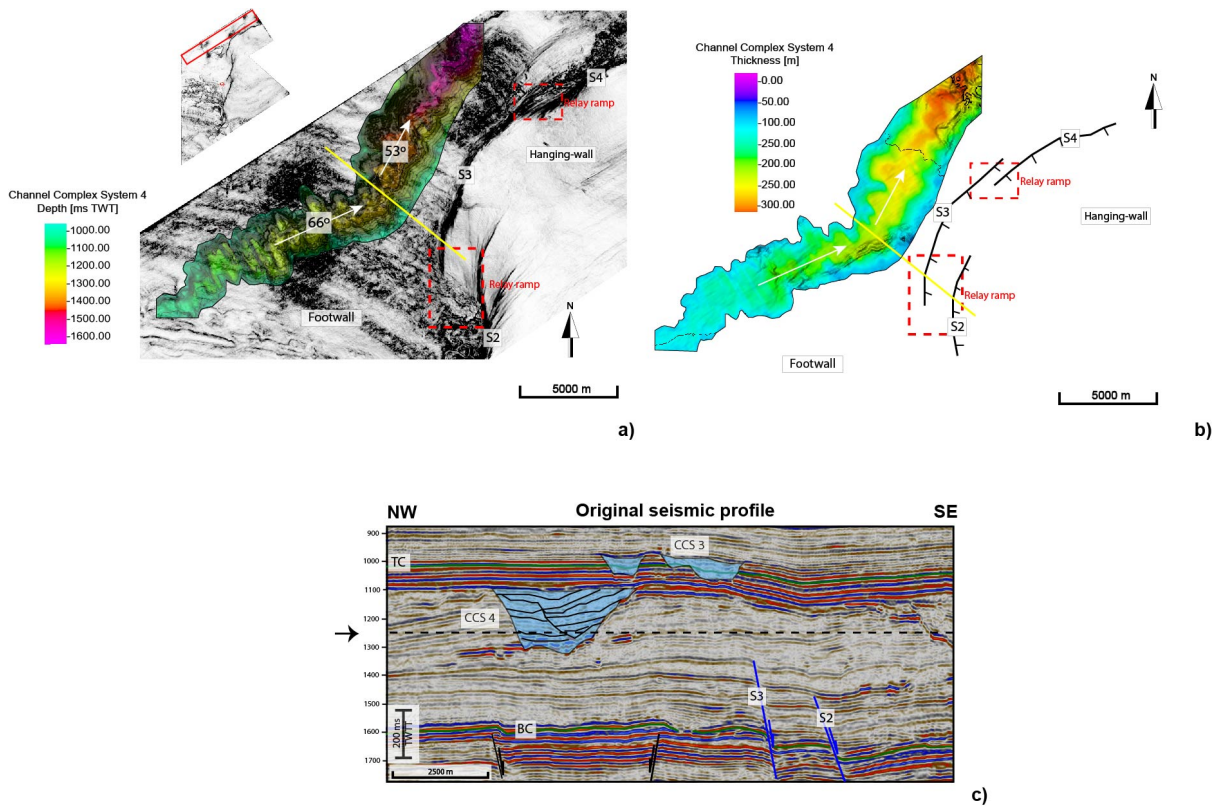
713

714

715

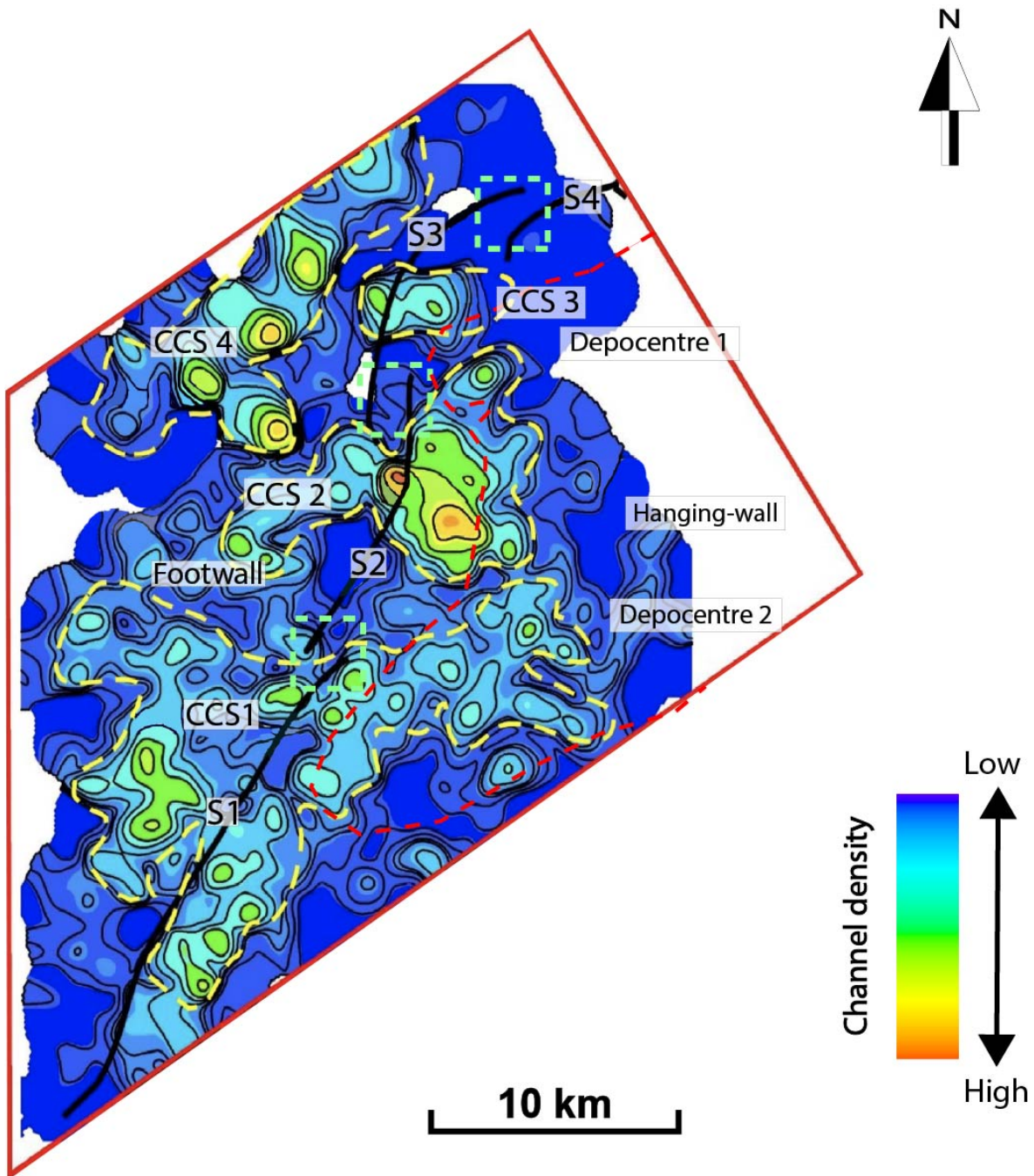
716

717



718

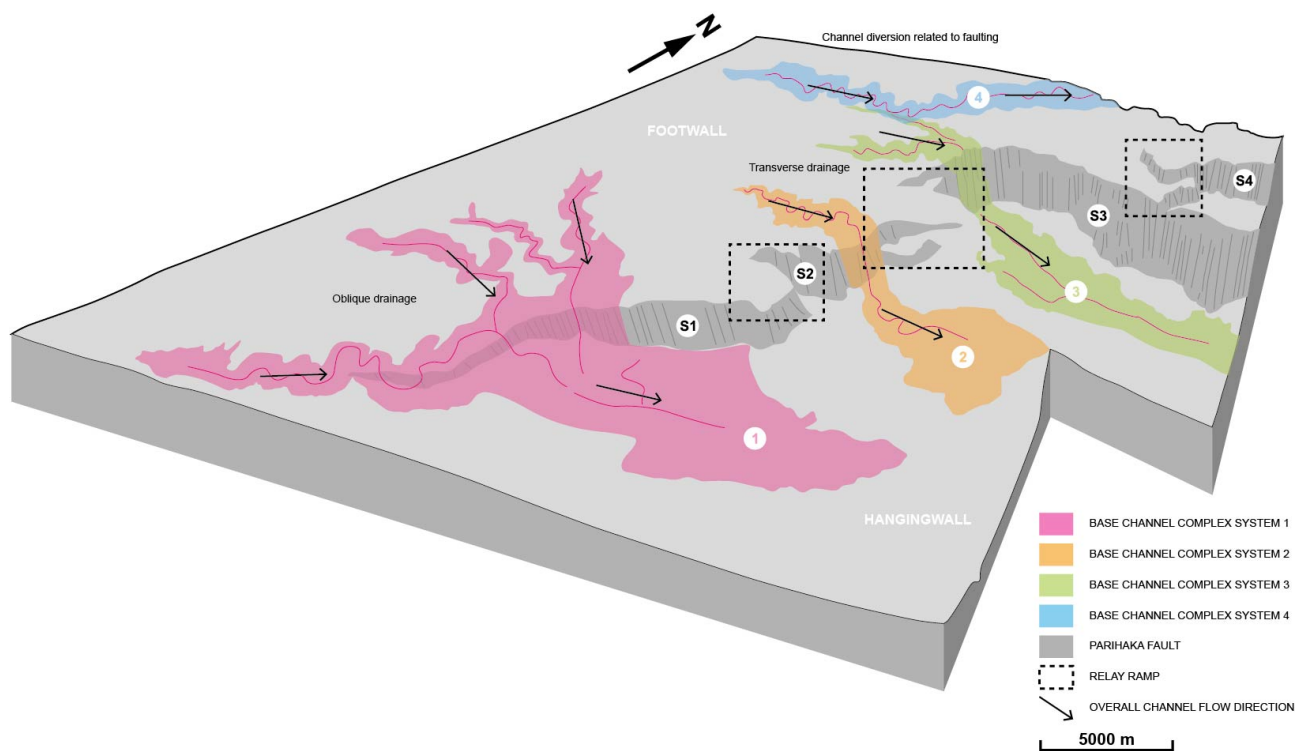
719 Figure 10: Detailed seismic interpretation of Channel Complex System 4 (CCS 4 in the boxes). a) Variance time-slice at  
 720 1320 ms showing the base of Channel Complex System 4 in the footwall block, the segments of Parihaka Fault, the  
 721 position of the seismic profile (yellow line), and the angles this channel system make to S3. b) Time-structural map for  
 722 Channel Complex System 4 showing the channel body flowing parallel to the Parihaka Fault trace. c) Selected seismic  
 723 profile highlighting the channel geometry relative to the Parihaka Fault. Channel Complex System 3 is also observed in  
 724 this seismic profile above horizon TC.



725

726 Figure 11: Channel point density plot showing the lateral and vertical stacking patterns of submarine channel complexes  
 727 (CCS in the boxes) in the study area. The main channel complex systems were delimited to this plot to facilitate the  
 728 analysis of the channel density distribution. The greatest channel point density occurs in the areas corresponding to  
 729 Channel Complex System 4 on the footwall block and Channel Complex System 2 on the hanging-wall block.

### CHANNEL DISTRIBUTION IN THE STUDY AREA



730

731 Figure 12: Block diagram summarising the channel distribution the study area indicating the three types of drainage  
 732 related to the Parihaka Fault trace. In the southern part of the study area, Channel Complex System 1 is an example of  
 733 oblique drainage, while Channel Complex Systems 2 and 3 in the central parts of the study area are an example of  
 734 transverse drainage related to a greater displacement of S2 and S3. Channel Complex System 4 is a channel that has  
 735 changed its course due to the uplift of the footwall block, running parallel to S3.